Supplementary Information (SI) for Journal of Materials Chemistry A.
This journal is © The Royal Society of Chemistry 2025

Supplementary Information

Bidirectional S-Bridge Coordination in Magnetic Au/FeO_xS_y Catalyst for the Catalytic Oxidation of 5-Hydroxymethylfurfural to 2,5-Furandicarboxylic Acid

Yu Ruan,[a] Shaoyi Wu, [a] Yingxin Lu, [a] Tiefeng Xu, *[ab] Wenxing Chen[ab] and Wangyang Lu[ab]

[a]State Key Laboratory of Bio-based Fiber Materials, Zhejiang Sci-Tech University, Hangzhou 310018, China

[b]Zhejiang Provincial Innovation Center of Advanced Textile Technology, Shaoxing 312000, China

Corresponding Author:

* E-mail: xutiefeng@zstu.edu.cn (T. Xu)

Tel: +86 571 86843611; Fax: +86 57186843611.

1. Materials

In this study, a range of chemicals and reagents were used for the experiments. These included chloroauric acid ($HAuCl_4 \cdot 4H_2O$, 99.95 %, Au > 47.8 %), sodium hydroxide (NaOH, AR), ferric chloride ($FeCl_3$), thiourea (CH_4N_2S), anhydrous sodium acetate ($C_2H_3NaO_2$), 5-hydroxymethyl-2-furaldehyde (HMF, 95 %), 5-formyl-2-furancarboxylic acid (HMFCA, 98 %), 5-Hydroxymethyl-2-furancarboxylic acid (FFCA, 98 %), 2,5-furandicarboxylic acid (FDCA, 98 %), sodium carbonate anhydrous, Triethylamine (Et_3N), isopropyl alcohol (IPA), p-benzoquinone(p-BQ), and L-histidine (L-His), all of which were sourced from Aladdin Chemical Co., Ltd. 5,5-dimethyl-1-pyrroline-N-oxide (DMPO), 2,2,6,6-tetramethyl-4-piperidinol (TEMP), and 2,2,6,6-tetramethyl-1-piperidinyloxy (TEMPO) were obtained from J&K Chemical Ltd. Ethylene glycol was obtained from McLean.

2. Characterization

Transmission electron microscopy (TEM) and high-resolution transmission electron microscopy (HRTEM) of the sample were conducted on a Bruker Nano GmbH Berlin microscopy at an acceleration voltage of 200 kV. A Bruker Nano GmbH Berlin microscopy equipped with an energy dispersive X-ray (EDS) detector was applied. The X-ray photoelectron spectroscopy (XPS, K-Alpha, Thermo, USA) with monochromatic Al Kα radiation (1486.6 eV) as the X-ray source was utilized. The powder X-ray diffraction (XRD, Empyrean) patterns of all samples were investigated using Empyrean

in the 2θ range of 10-90º with Cu Kα radiation.Electron paramagnetic resonance (EPR) was performed on a Bruker A300 spectrometer. The Raman spectrometer used was a Renishaw inVia Raman Microscope.

3. Liquid phase methods

Ultra Performance Liquid Chromatography (UPLC, Waters) method: The column temperature was set at 40 °C and the mobile phase was a mixture of methanol (solvent A) and water containing 0.1 % H_2SO_4 (solvent B). The intermediates were detected during the separation using an eluent gradient scheme: from 0 to 0.5 min, 5 % A; from 0.5 to 2.0 min, 5 % - 8 % A (linear); from 2.0 to 3.0 min, 8 % - 10 % A (linear); from 3.0 to 4.0 min, 10 % - 15 % A (linear); from 4.0 to 4.5 min, 15 % - 5 % A (linear); from 4.5 to 5.0 min, 5 % A (linear). The flow rate was 0.3 mL/min and the detection wavelengths of HMF, HMFCA, and FDCA were 285, 253, and 266 nm, respectively.

4. DFT calculations

All the DFT calculations were conducted based on the Vienna Ab-into Simulation Package (VASP) [1-2]. The exchange-correlation effects were described by the Perdew-Burke-Ernzerhof (PBE) functional within the generalized gradient approximation (GGA) method [3-4]. The core-valence interactions were accounted for by the projected augmented wave (PAW) method [5]. The energy cutoff for plane wave expansions was set to 400 eV. The structural optimization was completed for energy and force convergence set at 1.0×10^{-4} eV and 0.05 eV $Å^{-1}$, respectively. The Brillouin zone was

sampled with the 2×2×1 K-point. Grimme's DFT-D3 methodology[6] was used to describe the dispersion interactions.

The adsorption energies (E_{ads}) of HMF are calculated by

$$E_{ads} = E_{*HMF} - E_{HMF} - E_{Sub}$$

where E_{HMF} and E_{*HMF} represent the energies before and after the adsorption of HMF on the substrates, respectively. E_{sub} is the energy of Fe_3O_4-Au and Fe_3O_4-AuS surfaces.

The Gibbs free energy change (ΔG) of each step is calculated using the following formula:

$$\Delta G = \Delta E + \Delta ZPE - T\Delta S$$

where ΔE is the electronic energy difference directly obtained from DFT calculations, ΔZPE is the zero point energy difference, T is the room temperature (298.15 K) and ΔS is the entropy change. ZPE could be obtained after frequency calculation by [7]:

$$ZPE = \frac{1}{2}\sum hvi$$

And the TS values of adsorbed species are calculated according to the vibrational frequencies[8]:

$$TS = k_B T \left[\sum_k ln(\frac{1}{1 - e^{-hv/k_B T}}) + \sum_k \frac{hv}{k_B T} \frac{1}{(e^{hv/k_B T} - 1)} + 1 \right]$$

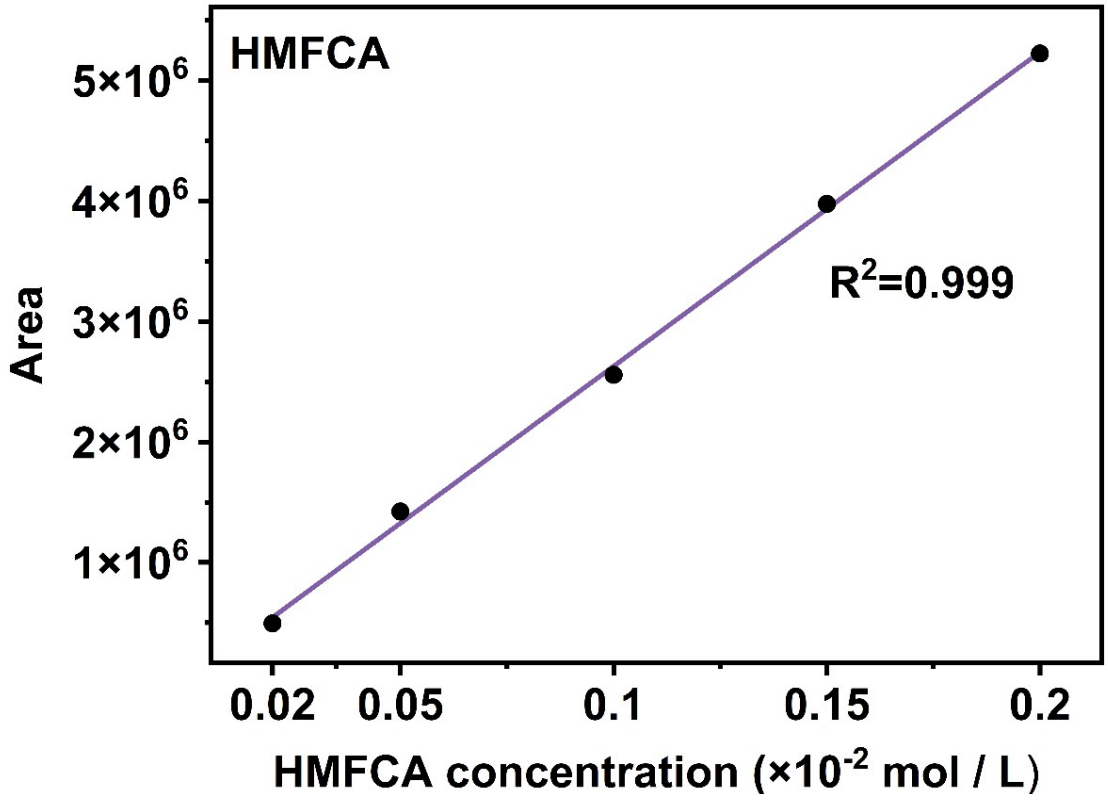

Fig. S1. Standardized graph of HMFCA.

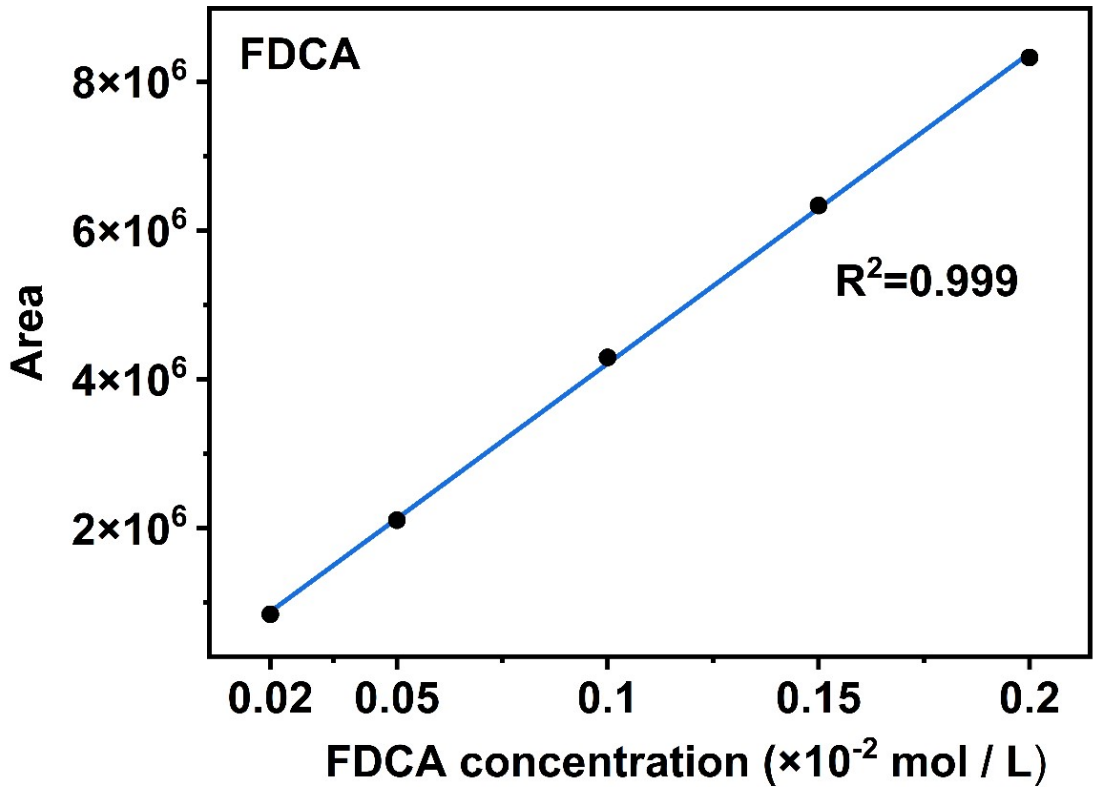

Fig. S2. Standardized graph of FDCA.

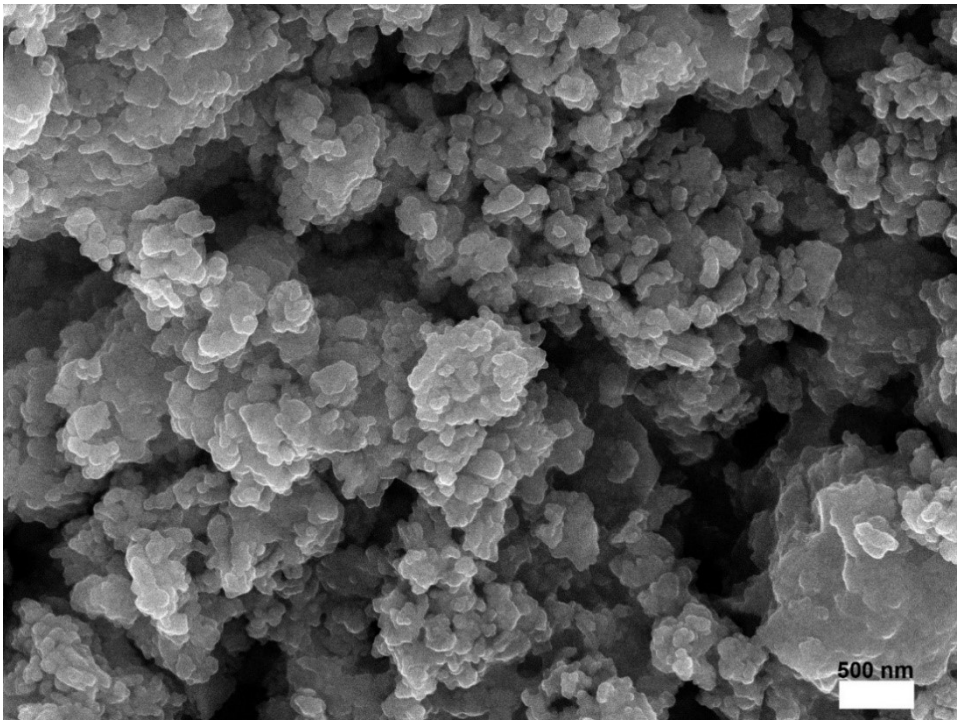

Fig. S3. SEM image of FeO_xS_y.

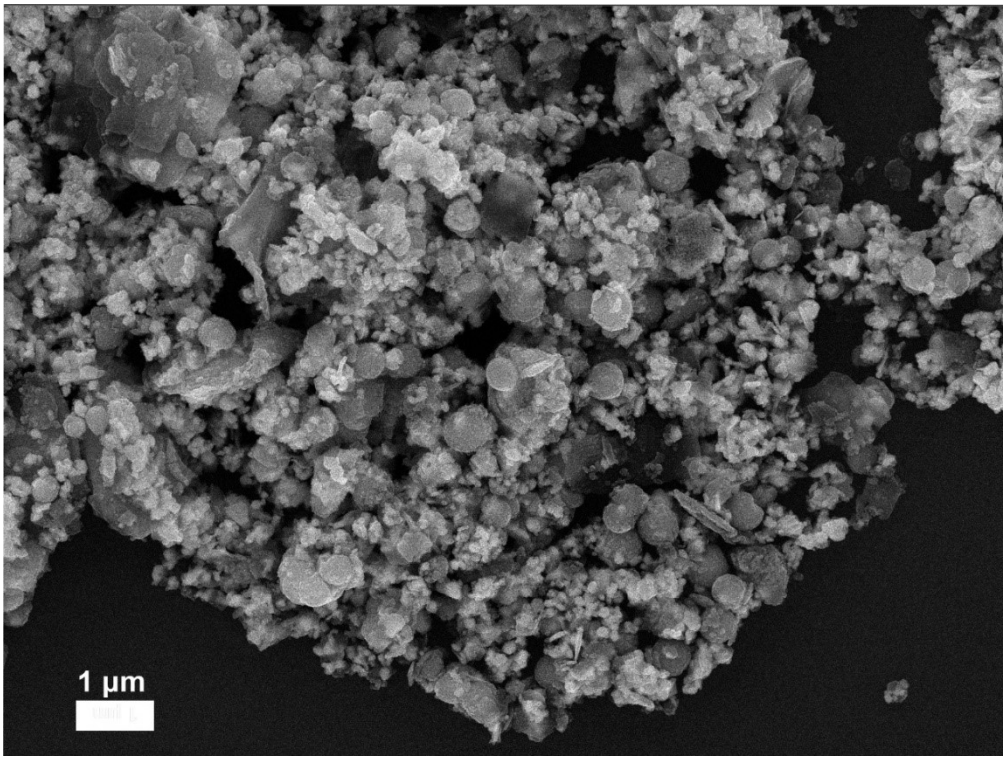

Fig. S4. SEM image of Au/FeO_xS_y-uncalcined.

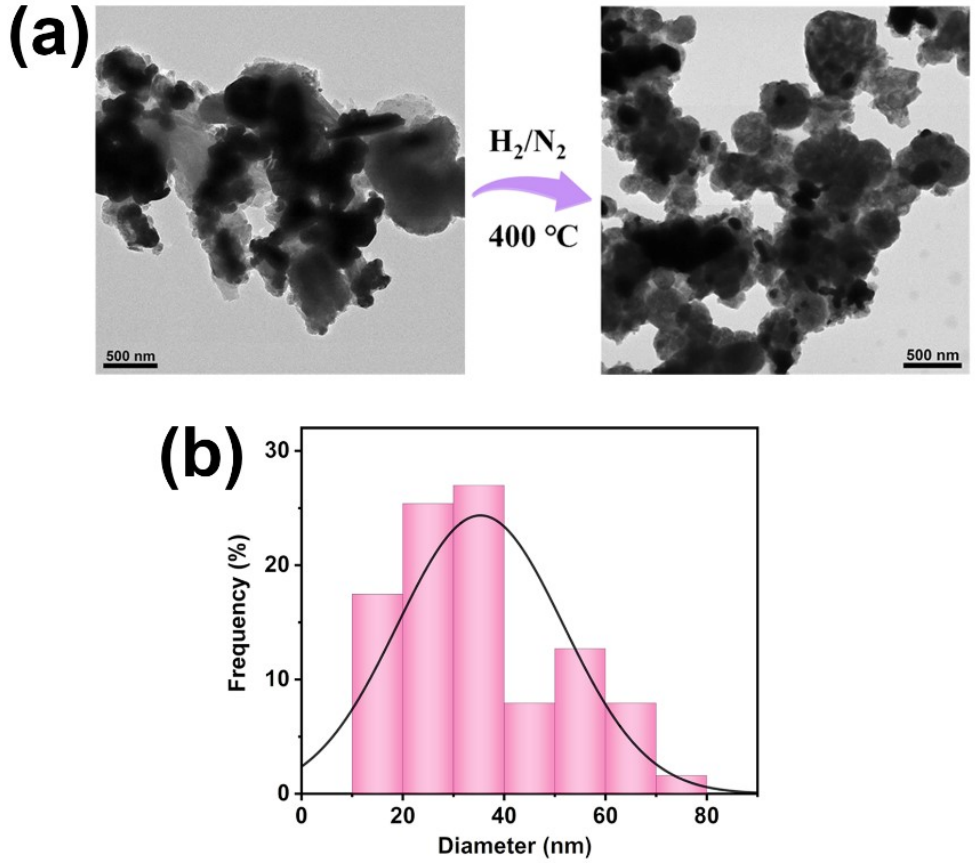

Fig. S5. (a) STEM comparison images before and after calcination. (b) Statistical analysis of Au particle size distribution of Au/FeO_xS_y.

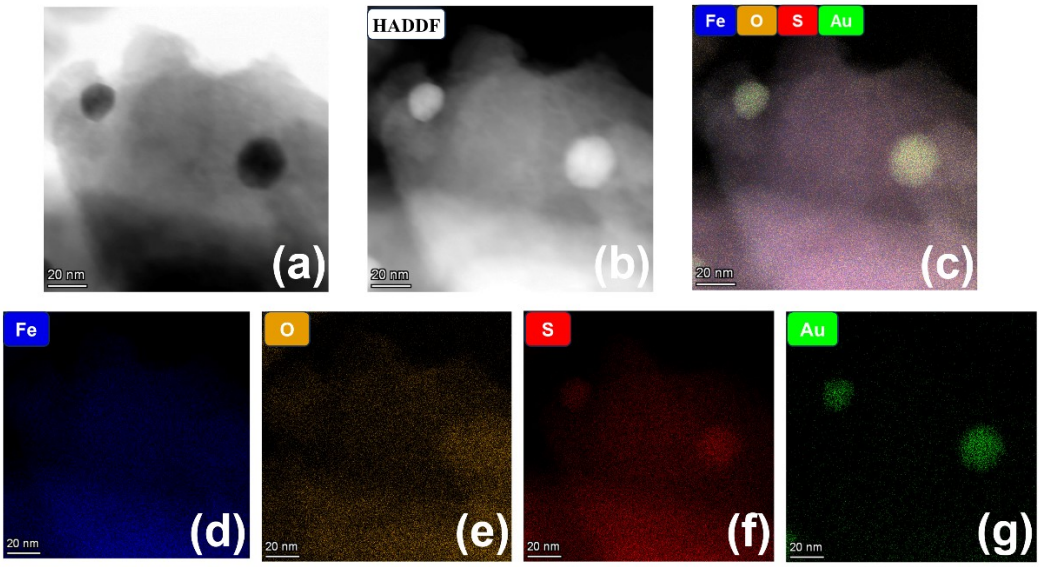

Fig. S6. (a) STEM image (b) HAADF-STEM image (c-g) Corresponding element mapping images of Au/FeO_xS_y-uncalined.

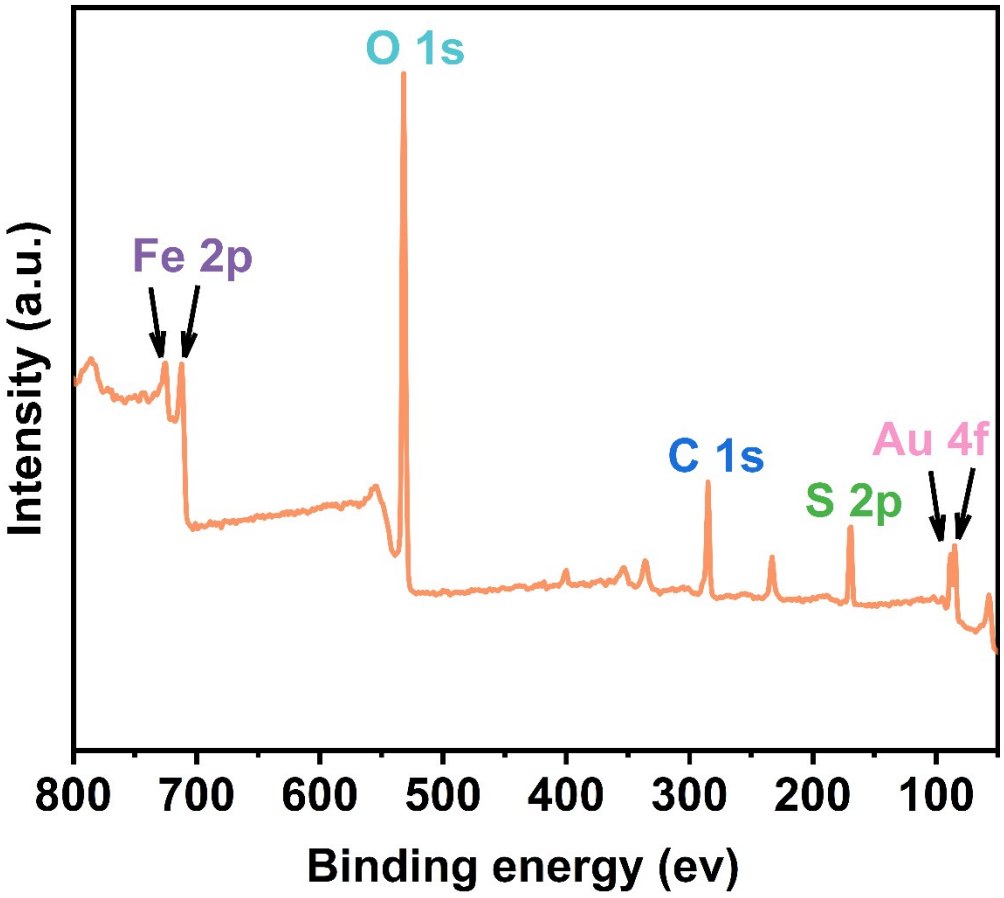

Fig. S7. XPS full-spectrum image.

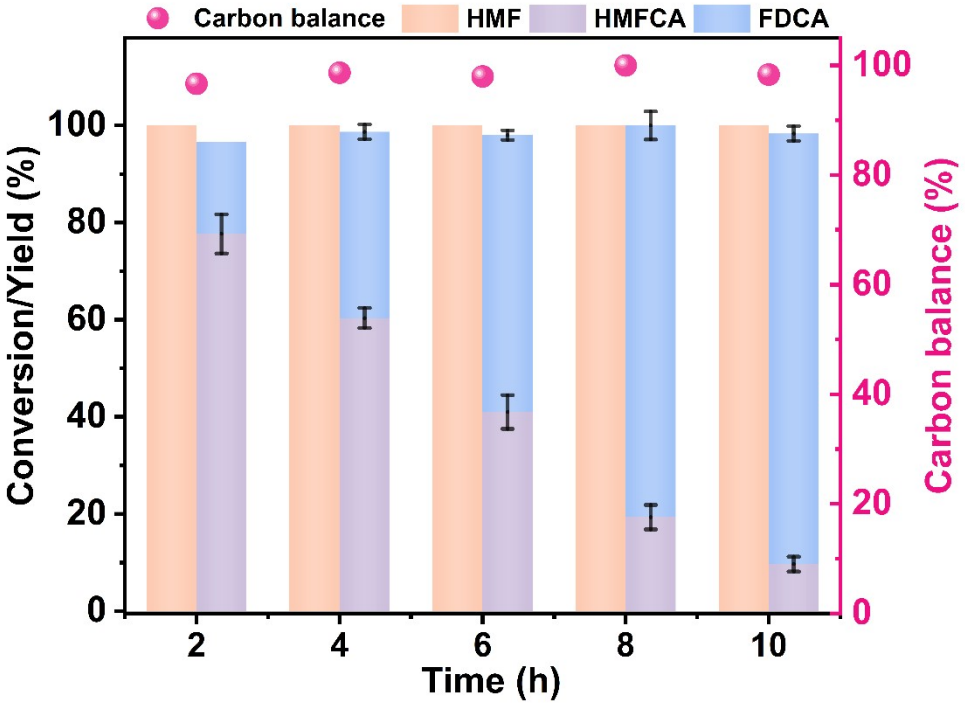

Fig. S8. Catalytic oxidation of HMF in the presence of Au/FeO_xS_y at 40°C. (Reaction conditions: 0.1 mmol HMF, 5 mL H_2O, *n*(Au)/*n*(Fe) = 0.5, 50 mg Catalyst, *n*(NaOH)/*n*(HMF) = 5).

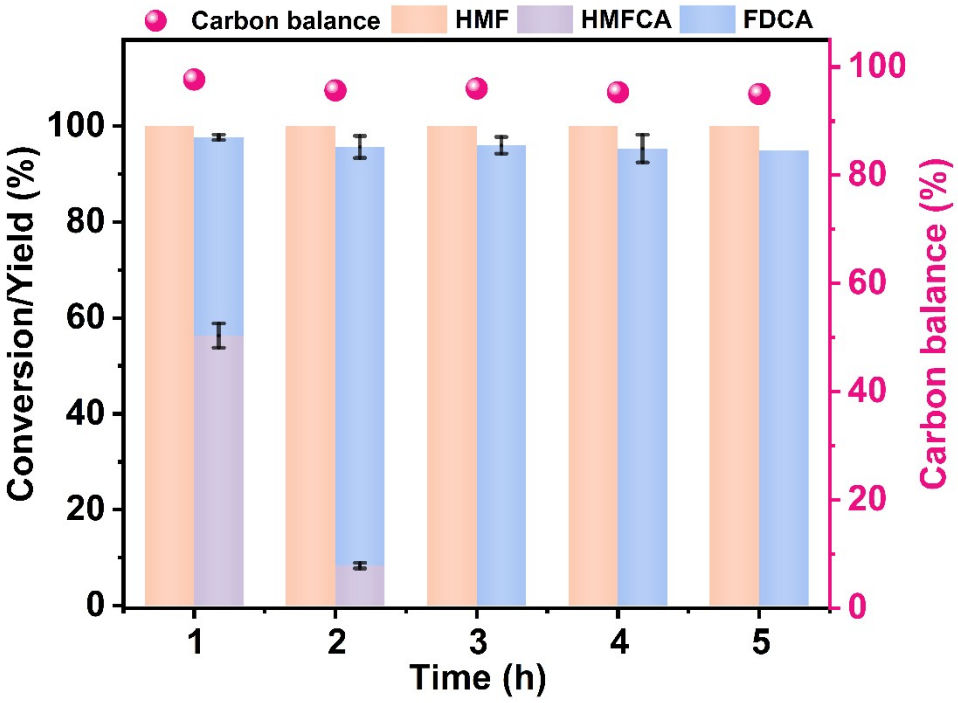

Fig. S9. Catalytic oxidation of HMF in the presence of Au/FeO_xS_y at 80°C. (Reaction conditions: 0.1 mmol HMF, 5 mL H_2O, *n*(Au)/*n*(Fe) = 0.5, 50 mg Catalyst, *n*(NaOH)/*n*(HMF) = 5).

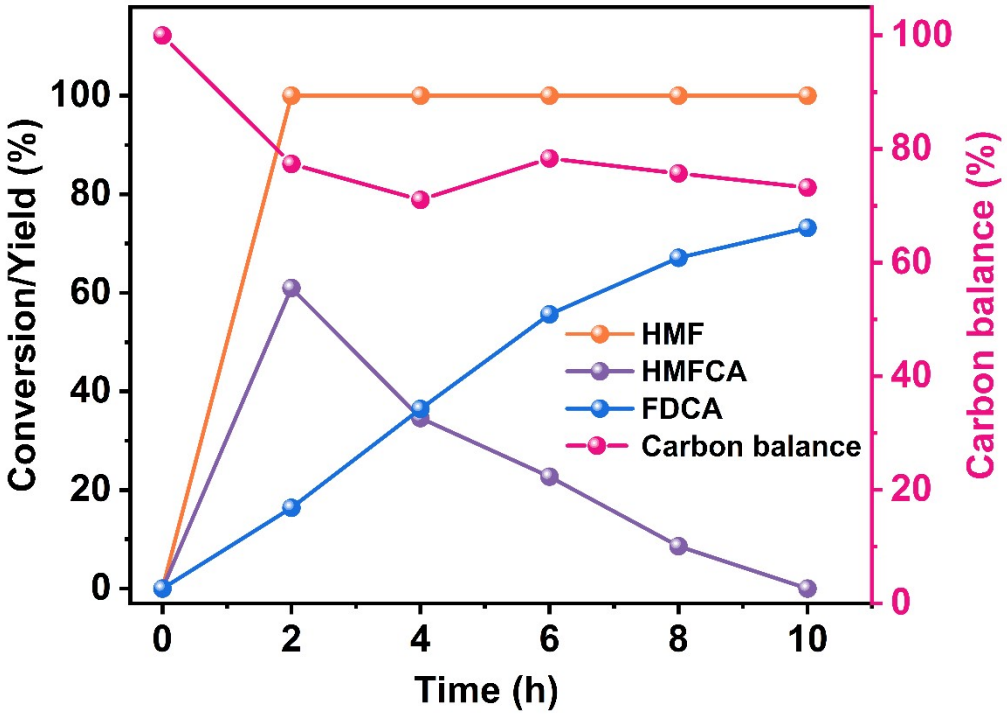

Fig. S10. Catalytic oxidation of HMF in the presence of Au/FeO_xS_y at 80°C. (Reaction conditions: 0.2 mmol HMF, 5 mL H_2O, *n*(Au)/*n*(Fe) = 0.5, 50 mg Catalyst, *n*(NaOH)/*n*(HMF) = 5).

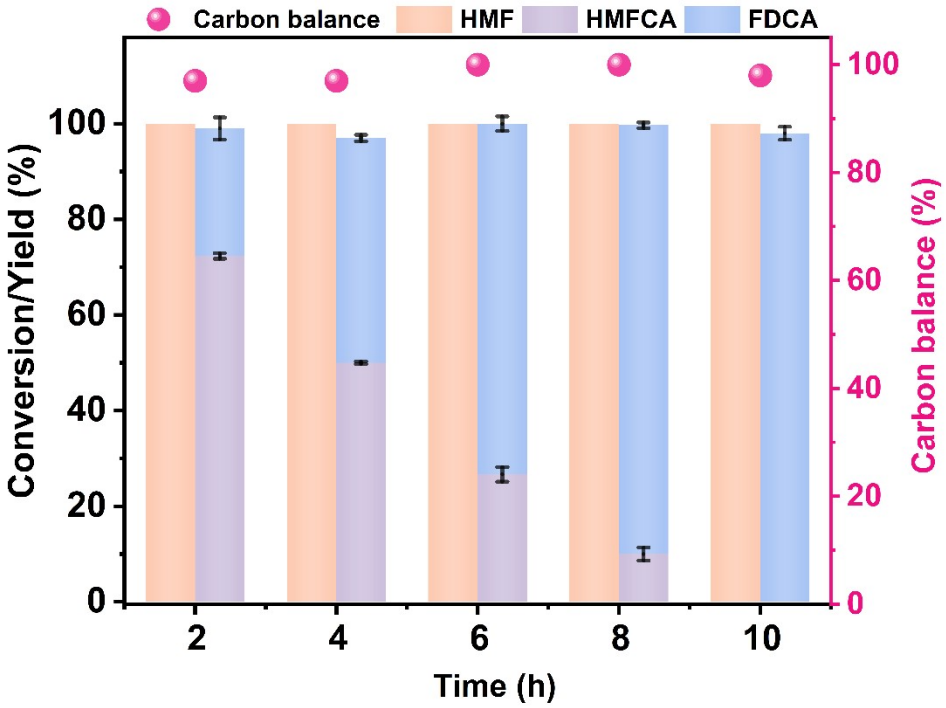

Fig. S11. Catalytic oxidation of HMF in the presence of the 30 mg Au/FeO_xS_y. (Reaction conditions: 0.1 mmol HMF, 5 mL H_2O, *n*(Au)/*n*(Fe) = 0.5, *n*(NaOH)/*n*(HMF) = 5:1, 60 °C).

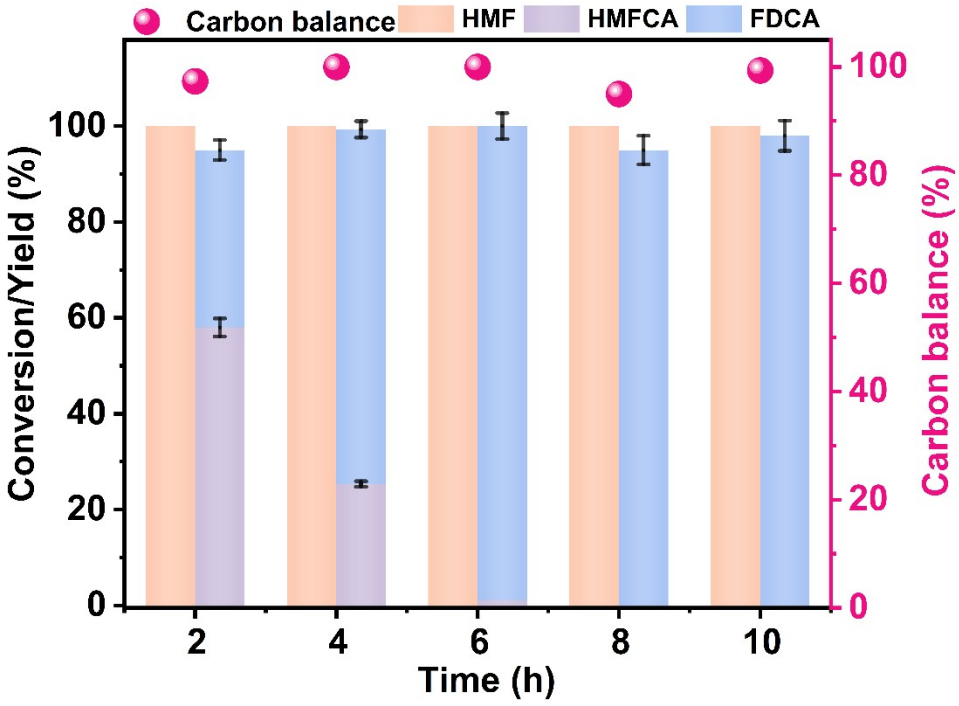

Fig. S12. Catalytic oxidation of HMF in the presence of the 40 mg Au/FeO_xS_y. (Reaction conditions: 0.1 mmol HMF, 5 mL H_2O, n(Au)/n(Fe) = 0.5, n(NaOH)/n(HMF) = 5:1, 60 °C).

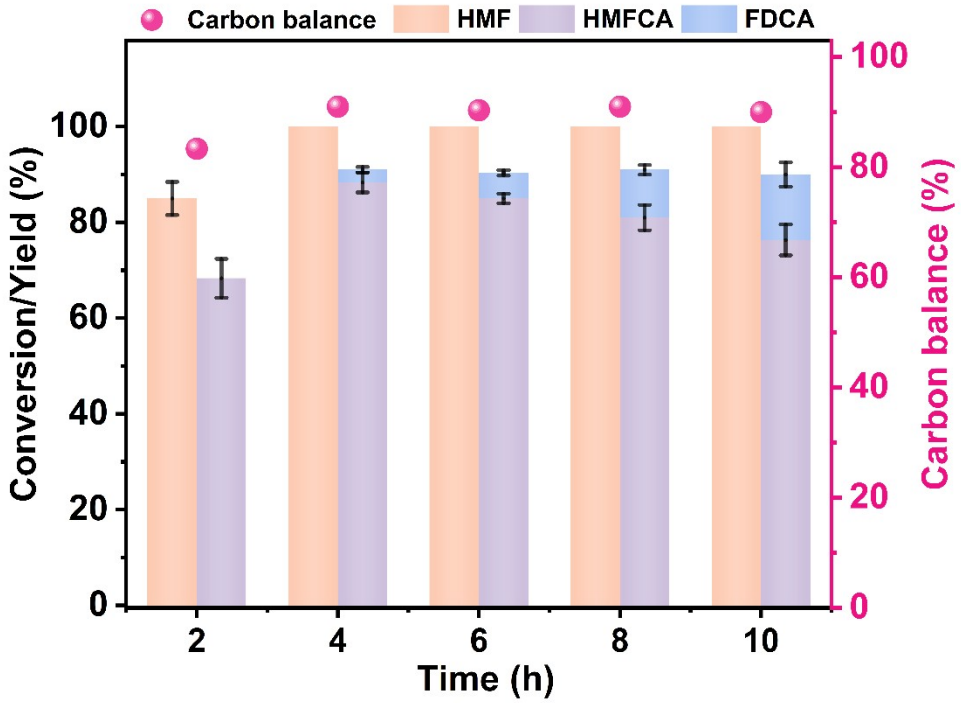

Fig. S13. Catalytic oxidation of HMF in the presence of Au/FeO_xS_y under N_2. (Reaction conditions: 0.1 mmol HMF, 5 mL H_2O, *n*(Au)/*n*(Fe) = 0.5, *n*(NaOH)/*n*(HMF) = 5:1, 60 °C).

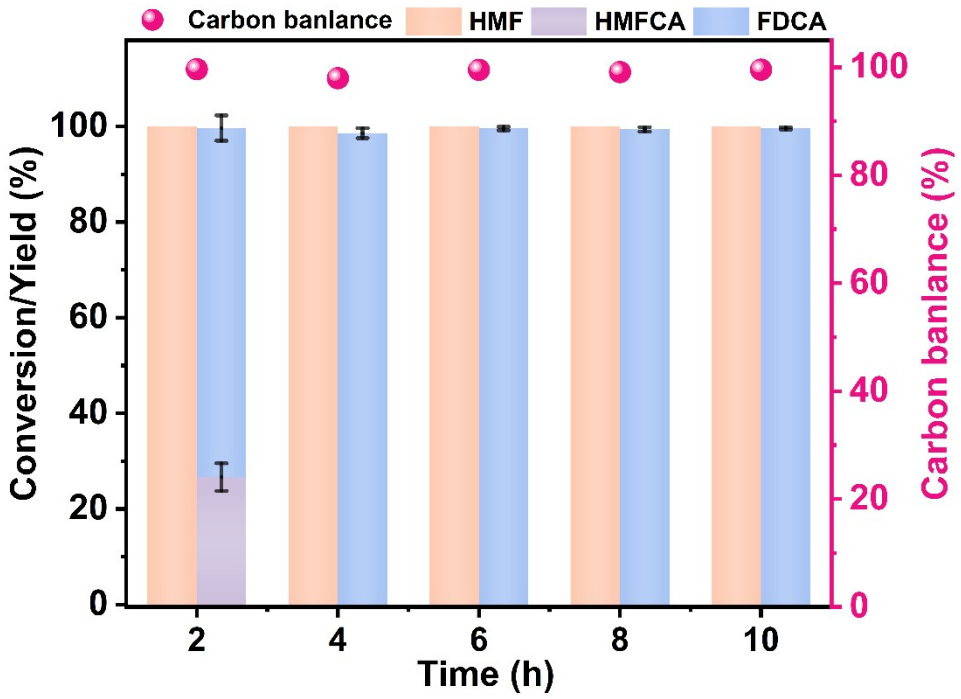

Fig. S14. Catalytic oxidation of HMF in the presence of Au/FeO_xS_y under O_2. (Reaction conditions: 0.1 mmol HMF, 5 mL H_2O, *n*(Au)/*n*(Fe) = 0.5, *n*(NaOH)/*n*(HMF) = 5:1, 60 ℃).

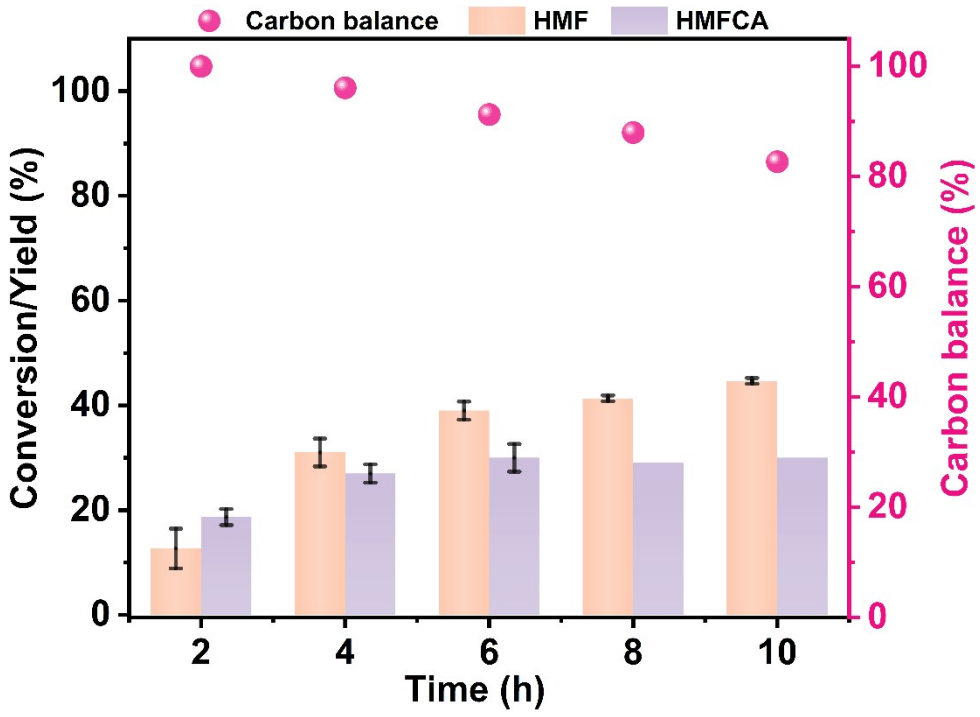

Fig. S15. Catalytic oxidation of HMF in the presence of Au/FeO_xS_y. (Reaction conditions: 0.1 mmol HMF, 5 mL H_2O, n(Au)/n(Fe) = 0.5, base-free, 60 °C).

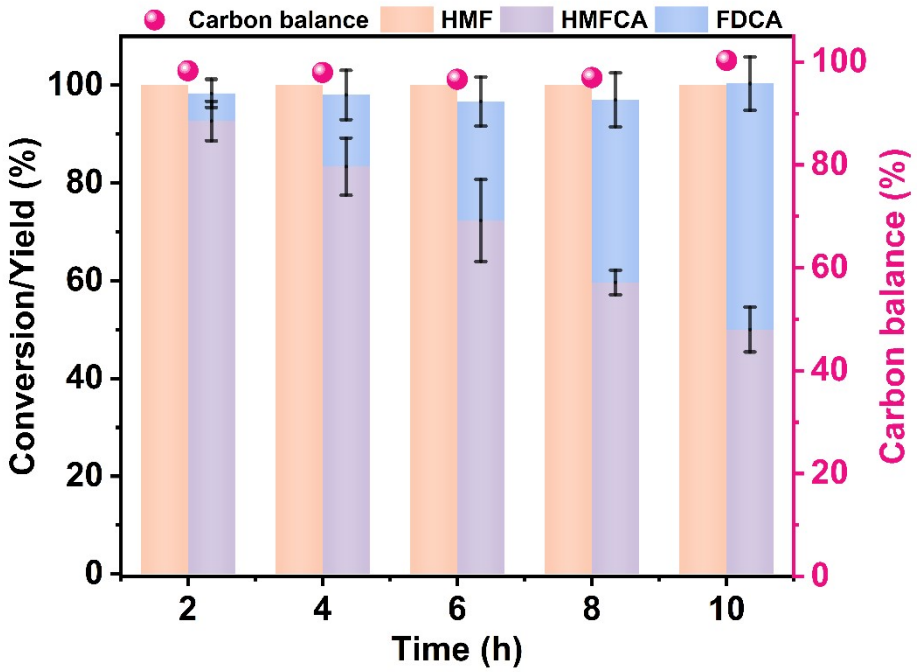

Fig. S16. Catalytic oxidation of HMF in the presence of Au/FeO_xS_y. (Reaction conditions: 0.1 mmol HMF, 5 mL H_2O, n(Au)/n(Fe) = 0.5, n($NaHCO_3$)/n(HMF) = 5:1, 60 °C).

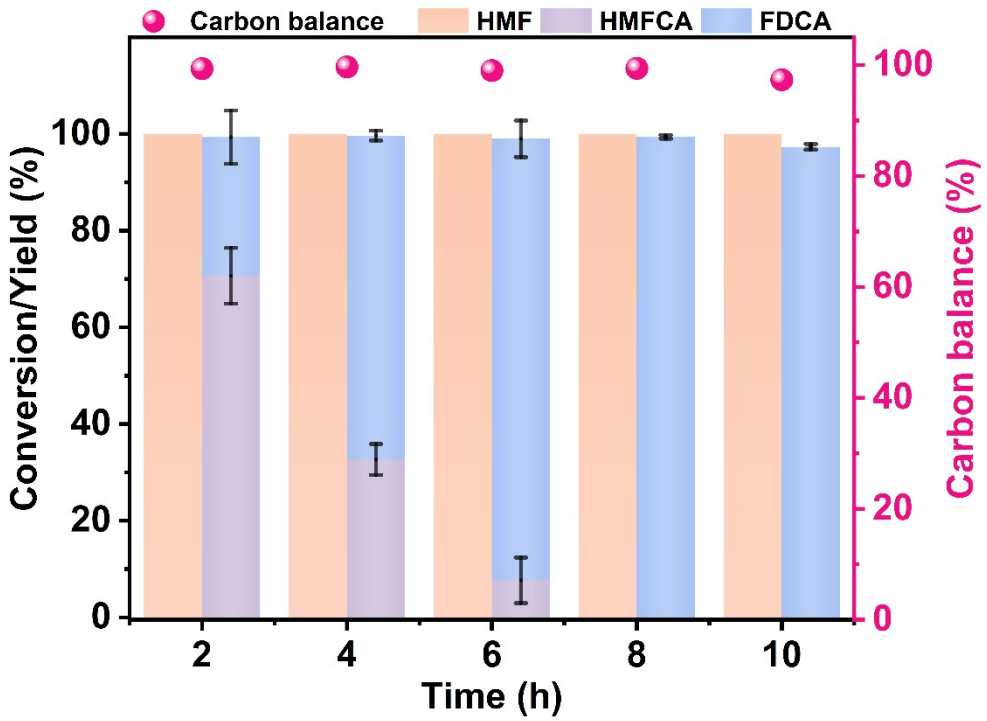

Fig. S17. Catalytic oxidation of HMF in the presence of Au/FeO_xS_y. (Reaction conditions: 0.1 mmol HMF, 5 mL H_2O, n(Au)/n(Fe) = 0.5, $n(Na_2CO_3)/n$(HMF) = 5:1, 60 °C).

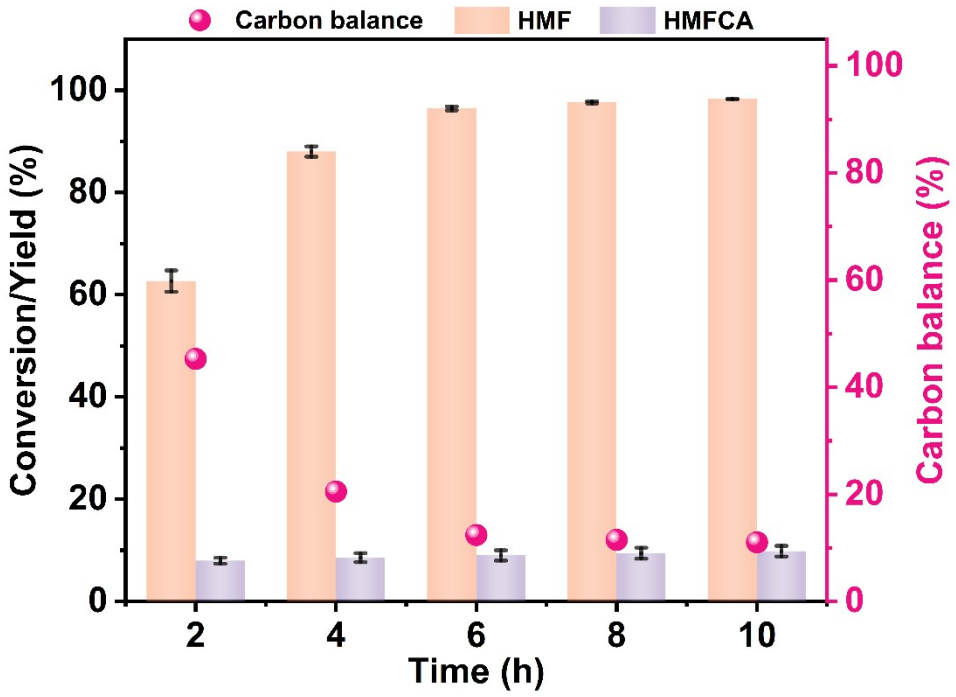

Fig. S18. Catalytic oxidation of HMF in the presence of Au/FeO_xS_y. (Reaction conditions: 0.1 mmol HMF, 5 mL H_2O, n(Au)/n(Fe) = 0.5, n(Et_3N)/n(HMF) = 5:1, 60 ℃).

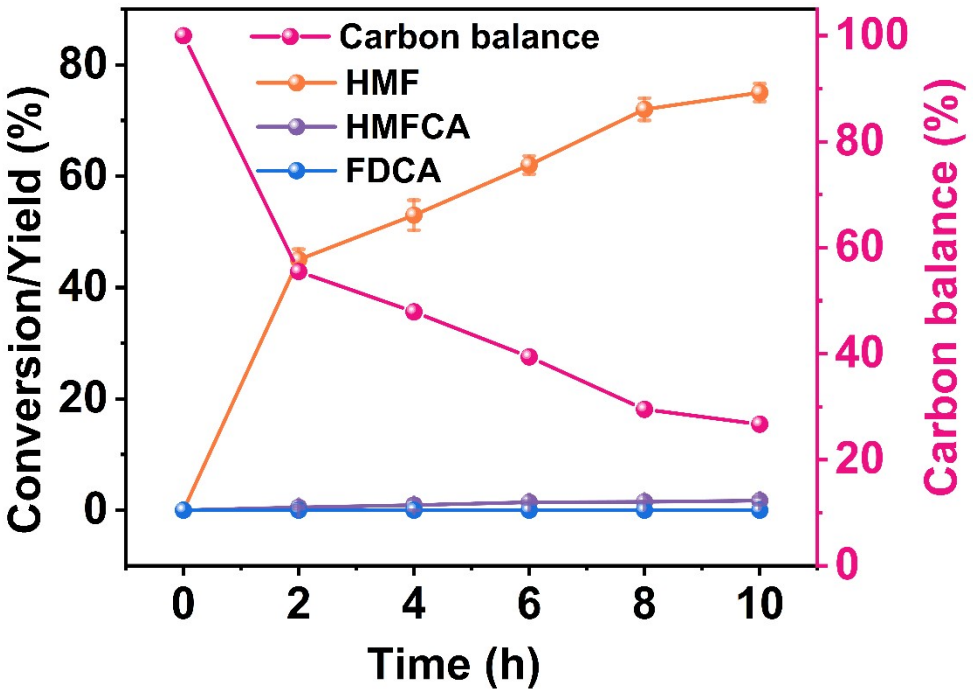

Fig. S19. Catalytic oxidation of HMF in the presence of FeO_xS_y. (Reaction conditions: 0.1 mmol HMF, 5 mL H_2O, *n*(Au)/*n*(Fe) = 0, *n*(NaOH)/*n*(HMF) = 5:1, 60 ℃).

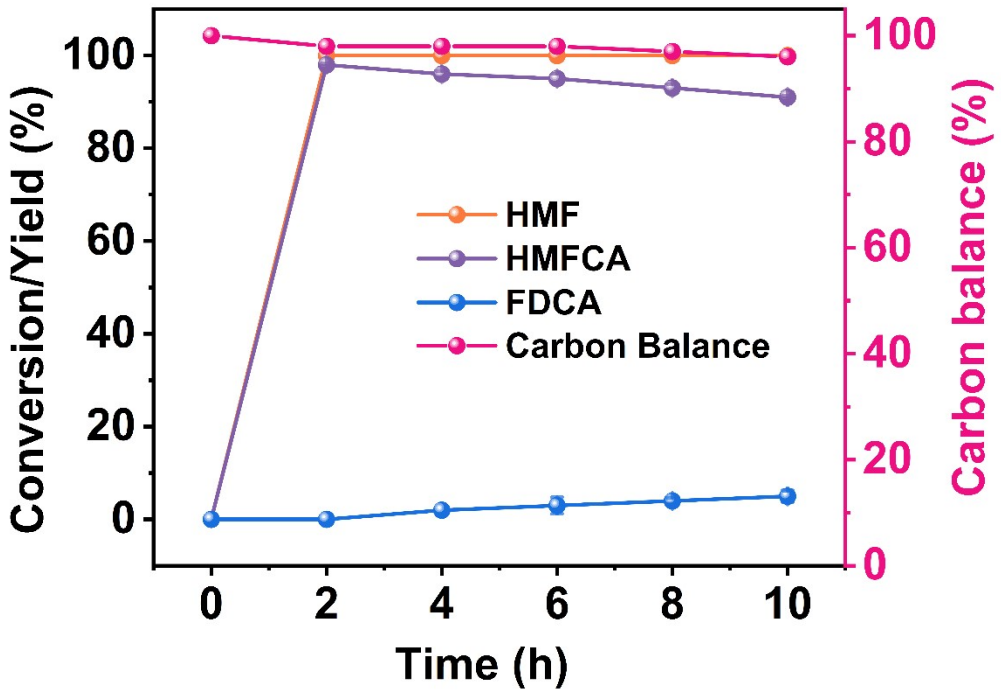

Fig. S20. Catalytic oxidation of HMF in the presence of Au/FeO_xS_y. (Reaction conditions: 0.1 mmol HMF, 5 mL H_2O, n(Au)/n(Fe) = 0.1, n(NaOH)/n(HMF) = 5:1, 60 ℃).

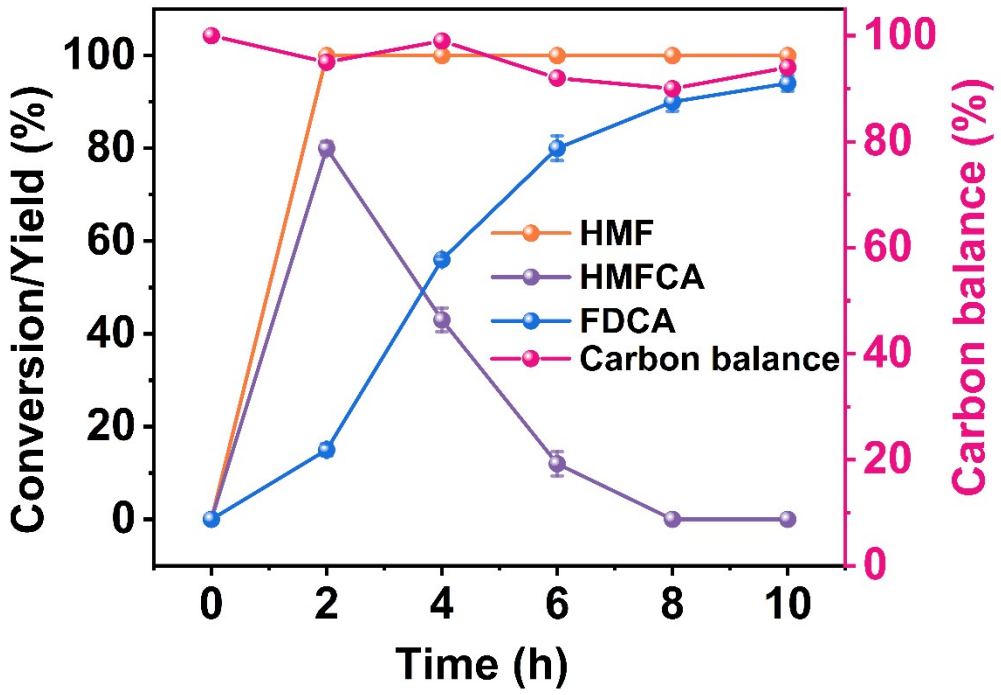

Fig. S21. Catalytic oxidation of HMF in the presence of Au/FeO_xS_y. (Reaction conditions: 0.1 mmol HMF, 5 mL H_2O, *n*(Au)/*n*(Fe) = 0.3, *n*(NaOH)/*n*(HMF) = 5:1, 60 ℃).

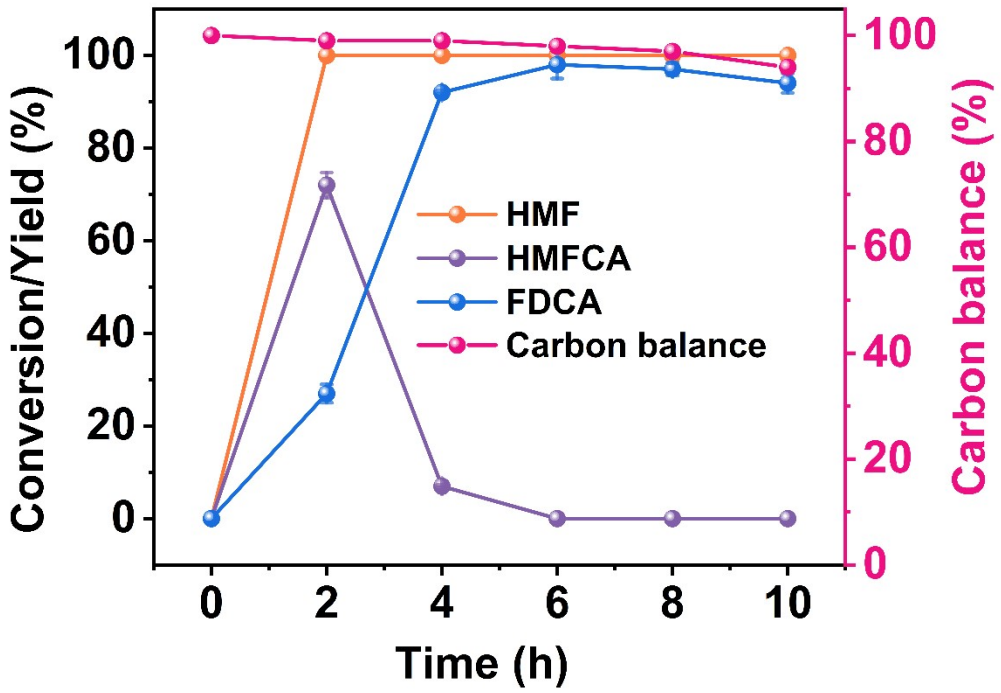

Fig. S22. Catalytic oxidation of HMF in the presence of Au/FeO_xS_y. (Reaction conditions: 0.1 mmol HMF, 5 mL H_2O, n(Au)/n(Fe) = 0.7, n(NaOH)/n(HMF) = 5:1, 60 ℃).

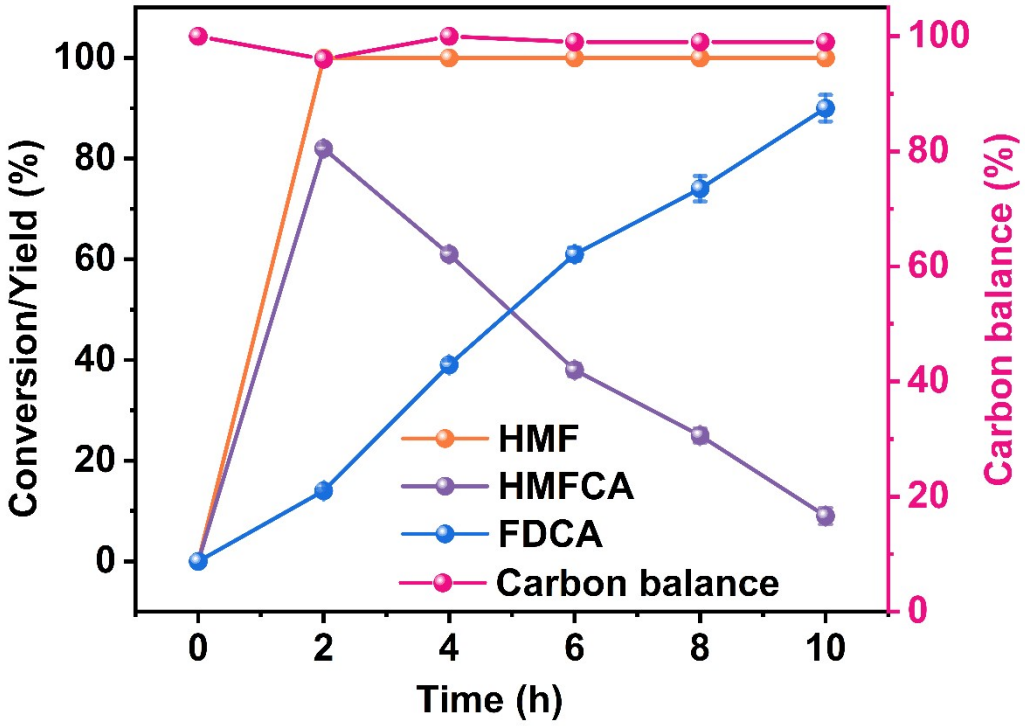

Fig. S23. Catalytic oxidation of HMF in the presence of Au/FeO_xS_y. (Reaction conditions: 0.2 mmol HMF, 5 mL H_2O, n(Au)/n(Fe) = 0.5, n(NaOH)/n(HMF) = 5:1, 60 ℃).

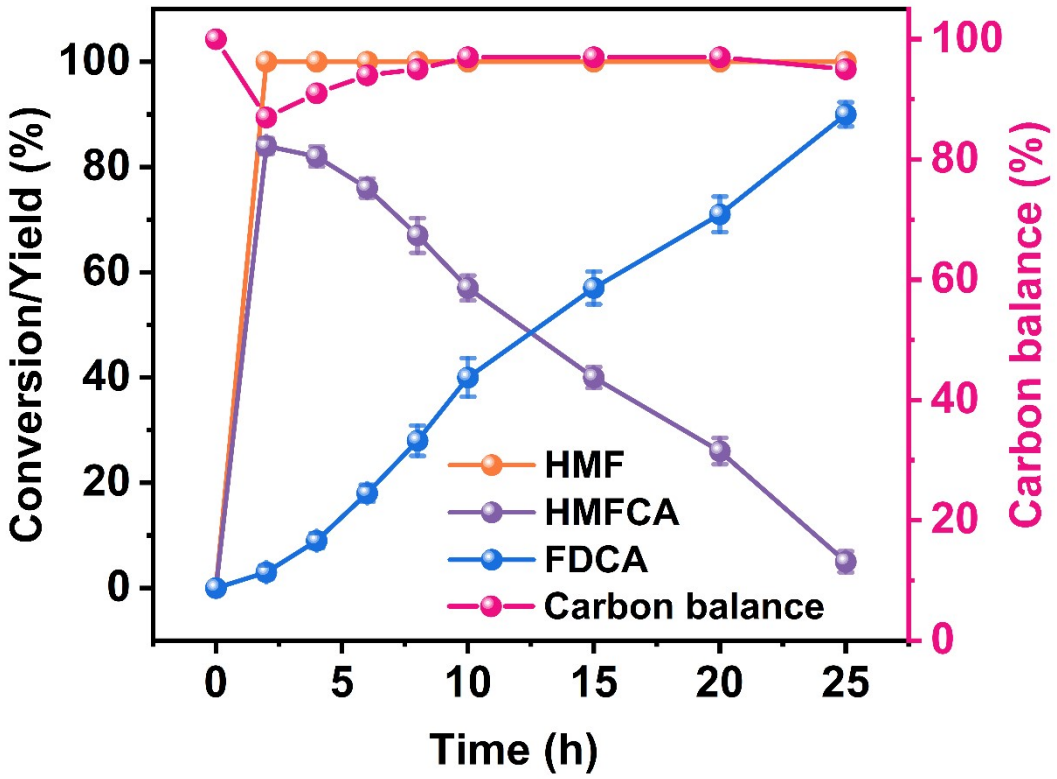

Fig. S24. Catalytic oxidation of HMF in the presence of Au/FeO_xS_y. (Reaction conditions: 0.4 mmol HMF, 5 mL H_2O, n(Au)/n(Fe) = 0.5, n(NaOH)/n(HMF) = 5:1, 60 °C).

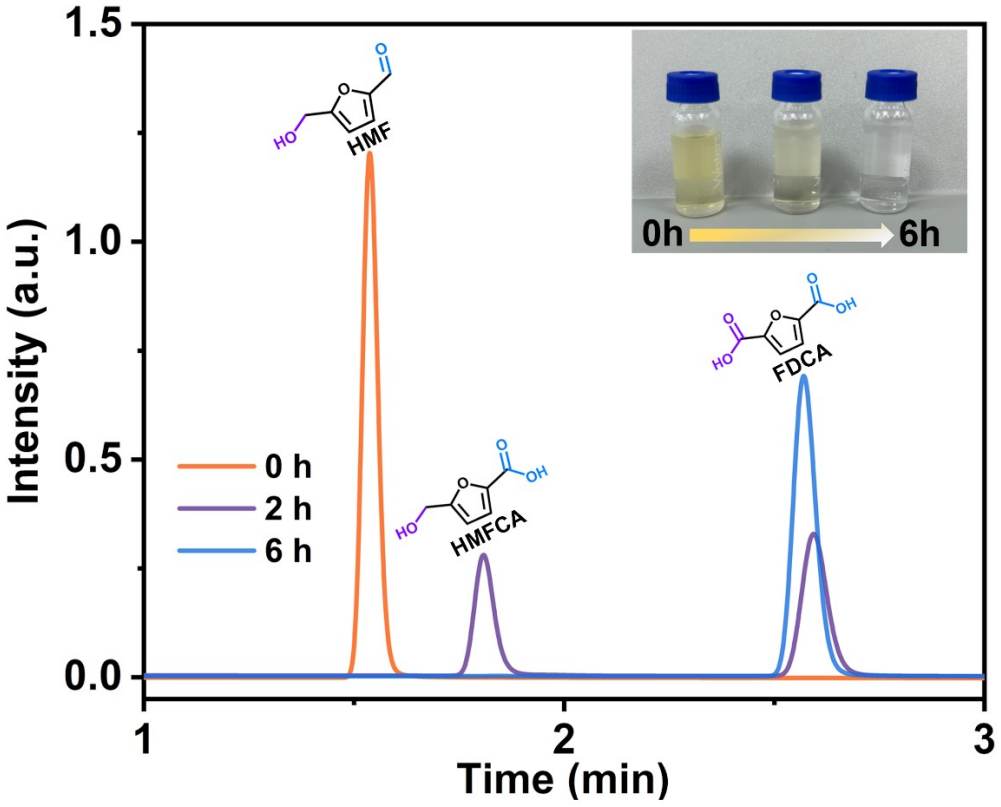

Fig. S25. Liquid chromatograms and changes in the color of the reaction solution.

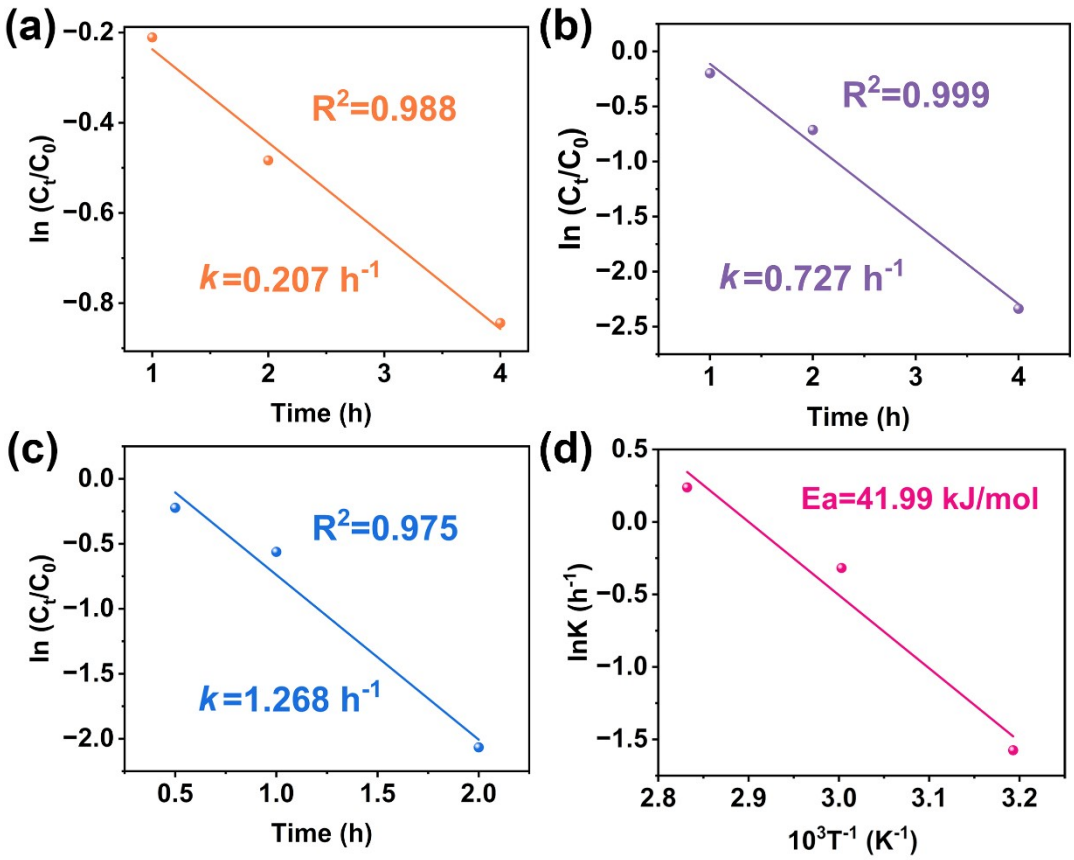

Fig. 26. Kinetic fitting curves of HMF oxidation to FDCA at (a) 40°C, (b) 60°C and (c) 80°C. (d) Arrhenius diagram for HMF oxidation to FDCA.

Table. S1. Compare the Ea values with other references.

Catalyst	Ea (kJ/mol)	Reference
Au/FeO_xS_y	41.99 (HMF→FDCA)	This Work
Au_2Pd_1/TiO_2-0.4CA@HNTs	78.9 (HMFCA→FDCA)	[9]
$Mn_6Ce_1O_x$	85.6 (HMF→FDCA)	[10]
Au_2Pd_1/CoO_x-HPC-500℃	87.2 (HMFCA→FDCA)	[11]
Au_3Pd_1/HRN_5C	138.5 (HMFCA→FDCA)	[12]

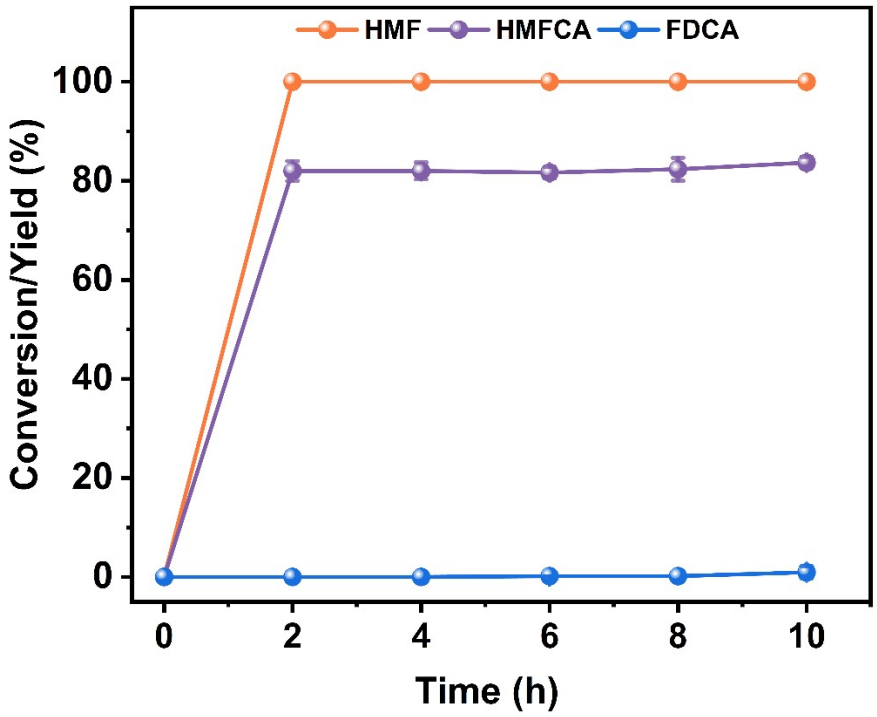

Fig. S27. Catalytic oxidation of HMF in the presence of Au/FeO_xS_y. (Reaction conditions: 0.1 mmol HMF, 0.1 mmol p-BQ, 5 mL H_2O, n(Au)/n(Fe) = 0.5, n(NaOH)/n(HMF) = 5:1, 60 °C).

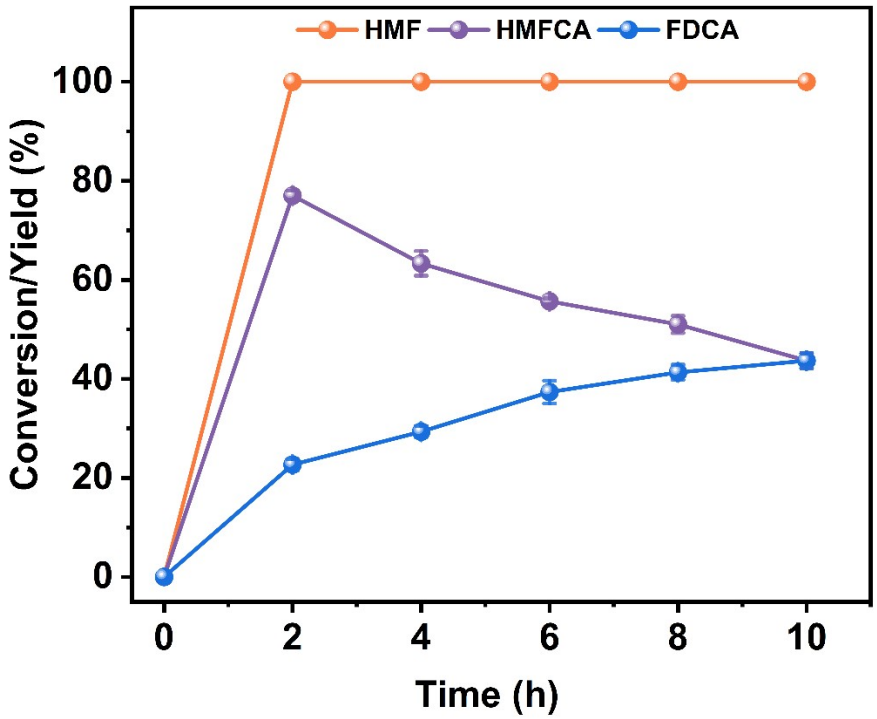

Fig. S28. Catalytic oxidation of HMF in the presence of Au/FeO_xS_y. (Reaction conditions: 0.1 mmol HMF, 0.1 mmol IPA, 5 mL H_2O, n(Au)/n(Fe) = 0.5, n(NaOH)/n(HMF) = 5:1, 60 °C).

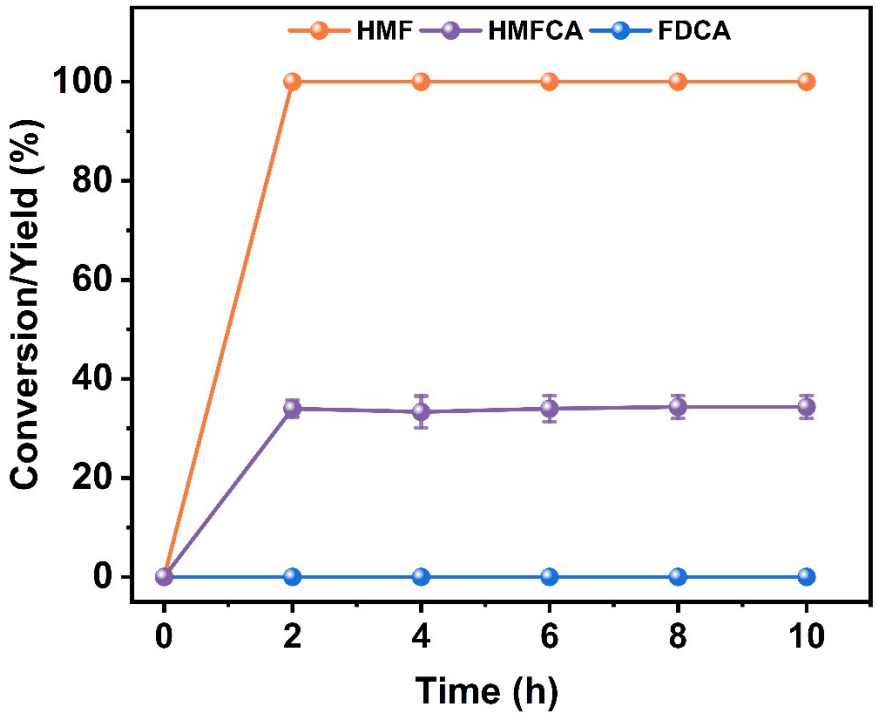

Fig. S29. Catalytic oxidation of HMF in the presence of Au/FeO_xS_y. (Reaction conditions: 0.1 mmol HMF, 0.1 mmol L-his, 5 mL H_2O, n(Au)/n(Fe) = 0.5, n(NaOH)/n(HMF) = 5:1, 60 °C).

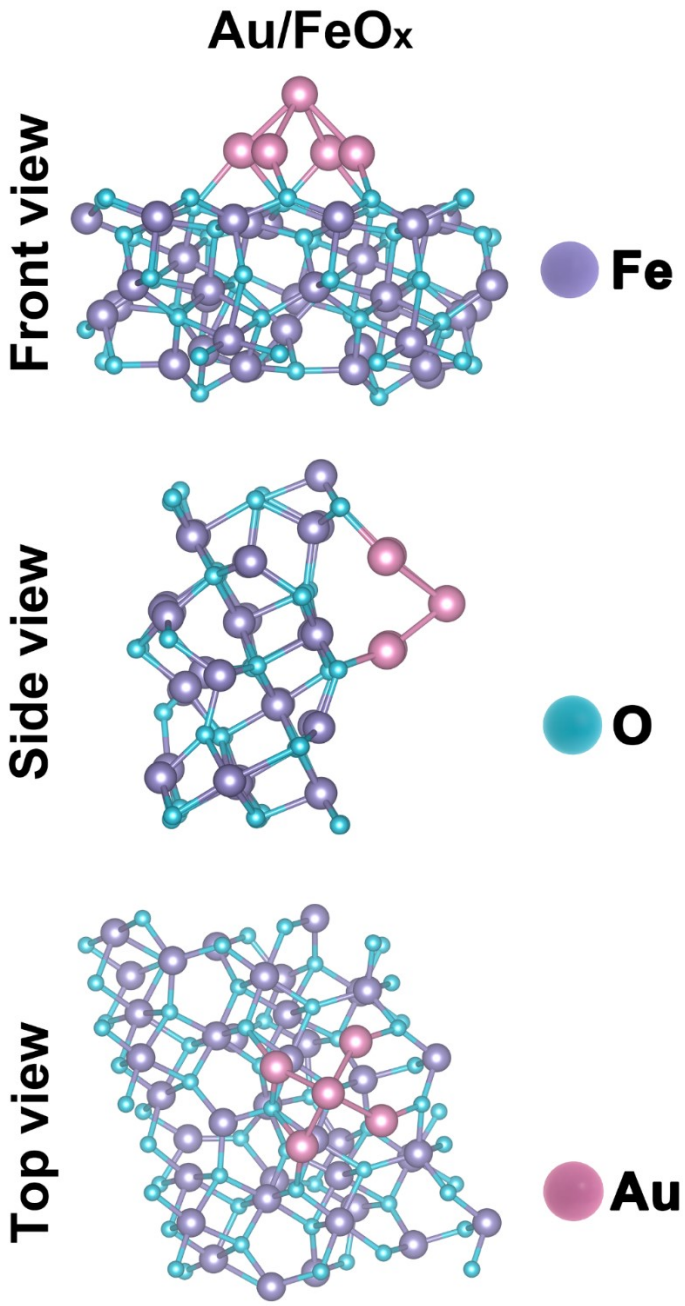

Fig. S30. Au/FeO_x catalyst after optimization.

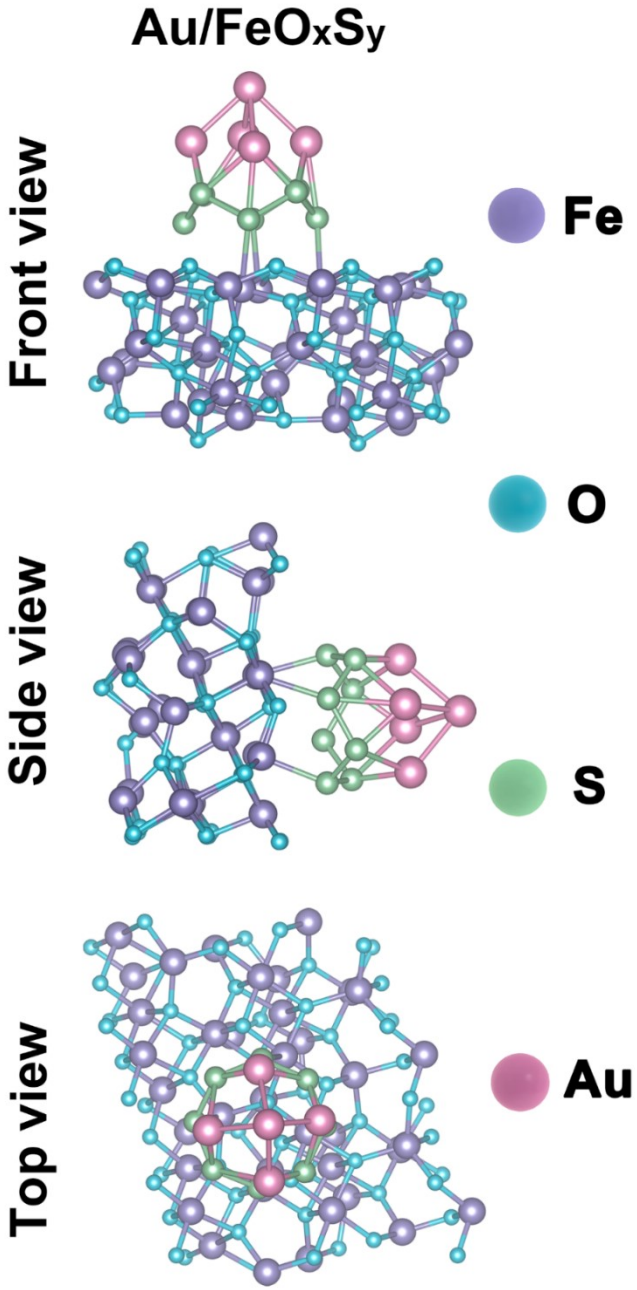

Fig. S31. Au/FeO_xS_y catalyst after optimization.

References

1 G. Kresse, J. Hafner, *Phys. Rev. B* 1993, **47**, 558-561.

2 G. Kresse, J. Hafner, *Phys. Rev. B* 1997, **49**, 14251-14269.

3 J. -P. Perdew, K. Burke, M. Ernzerhof, *Phys. Rev. Lett.* 1996, **77**, 3865-3868.

4 G. Kresse, D. Joubert, *Phys. Rev. B* 1999, **59**, 1758-1775.

5 P. -E. Blöchl, *Phys. Rev. B* 1994, **50**, 17953-17979.

6 S. Grimme, J. Antony, S. Ehrlich, H. Krieg, *J. Chem. Phys*. 2010, **132**, 154104.

7 J.-K. Nørskov, J. Rossmeisl, A. Logadottir, L. Lindqvist, J.-R. Kitchin, T. Bligaard, H. Jonsson, *J. Phys. Chem. B* 2004, **108**, 46, 17886–17892.

8 L.-I. Bendavid, E.-A. Carter, *J. Phys. Chem. C* 2013, **117**, 49, 26048–26059.

9 Y. Liu, Y. Chen, Y. Li, W. Guan, Q. Xia, M. Cao, P. Huo, Y. Zhang, *Chem. Eng. J.* 2023, **476**, 146874.

10 Q. Liu, Y. Gong, J. Zeng, Y. Zhao, J. Lv, Z. Jiang, C. Hu, Y. Zhou, *ACS Sustainable Chem. Eng.* 2025, **13**, 2107–2119.

11 W. Guan, C. Chen, B. Li, Y. Chen, Y. Wei, Y. Cao, F. Wang, Y. Yan, B. Liu, Y. Zhang, *ChemistrySelect* 2022,**7**, e202104058.

12 F. Wang, C. Yan, R. Jiang, Y. Chen, Y. Wei, Y. Cao, W. Guan, P. Huo, Y. Zhang, *Appl. Clay Sci.* 2023, **235**, 106872.